Curvelet-domain matched filtering

Felix J. Herrmann and Peyman P. Moghaddam* EOS-UBC, and Deli Wang†, Jilin University*

SUMMARY

Matching seismic wavefields and images lies at the heart of many pre-/post-processing steps part of seismic imaging—whether one is matching predicted wavefield components, such as multiples, to the actual to-be-separated wavefield components present in the data or whether one is aiming to restore migration amplitudes by scaling, using an image-to-remigrated-image matching procedure to calculate the scaling coefficients. The success of these wavefield matching procedures depends on our ability to (i) control possible overfitting, which may lead to accidental removal of energy or to inaccurate image-amplitude corrections, (ii) handle data or images with nonunique dips, and (iii) apply subsequent wavefield separations or migraton amplitude corrections stably. In this paper, we show that the curvelet transform allows us to address all these issues by imposing smoothness in phase space, by using their capability to handle conflicting dips, and by leveraging their ability to represent seismic data and images sparsely. This latter property renders curvelet-domain sparsity promotion an effective prior.

INTRODUCTION

Matched filtering for the purpose of matching the amplitudes of wavefields prior subtraction has been an integral part of the seismic data processor's toolbox (see e.g. Verschuur et al., 1992, where matched-filtering is used within Surface-Related Multiple Elimination, SRME). The recent advent of scaling methods for the restoration of migration amplitudes through image-to-remigrated-image matching (see e.g. Guitton, 2004; Herrmann et al., 2008a; Symes, 2008) represent another instance of matched filtering.

Even though matched-filtering procedures have been applied successfully for cases where the data sets differ by only a single short convolutional filter, extensions of this framework to situations where the differences vary non stationarily has been more problematic. In this paper, we propose a method correcting for these nonstationary effects by making the following assumptions: (i) the stationary difference is removed by a global matching procedure, which corresponds to removal of the source/receiver directivity during primary-multiple separation (Herrmann et al., 2008b) or to making the migration operator zero-order during migration (see Herrmann et al., 2008a, and another contribution by the authors to the proceedings of this conference), and (ii) the remaining non-stationary difference is assumed to vary smoothly in phase space—i.e., the amplitude mismatches are assumed to vary smoothly as a function of position and dip along coherent wavefronts.

THE FORWARD MODEL

Under above assumptions, the nonstationary 'scaling' can be represented mathematically by a zero-order pseudo-differential operator (ΨDO), whose action on an arbitrary d-dimensional function is given by

$$\big(Bf\big)(x) = \int_{x\in\mathbb{R}^d} e^{jk\cdot x} b(x,k)\hat{f}(k)\mathrm{d}k \qquad (1)$$

with k the wavenumber vector and $b(x,k)$ a space- and spatial-frequency dependent filter, known as the symbol. For our application, this operator acts either on shot records or on common-offset panels ($d = 2$) and applies a location, frequency, and dip-dependent scaling. After discretization, this operator models the mismatch by applying a matrix-vector multiplication —i.e.,

$$\mathbf{g} = \boldsymbol{B}\mathbf{f}, \qquad (2)$$

where $\boldsymbol{B}$ is a full positive-definite matrix, implementing the action of the pseudo-differential operator, and $\mathbf{f}$ and $\mathbf{g}$ the two to be matched discretized wavefields.

Image-to-remigrated-image matching: During seismic image-amplitude recovery, the above forward model is directly related to the fact that the demigration-migration operator can in the high-frequency limit be modeled by a ΨDO (Herrmann et al., 2008a). In that case, the vectors $\mathbf{f}$ and $\mathbf{g}$, represent the reference vector (say the migrated image) and the remigrated image (modeled and subsequently migrated reference image). For smooth velocity models, the symbol of this ΨDO is known to vary smoothly as function of space and spatial frequency.

Multiple-to-multiple matching: As part of matched filtering during primary-multiple separation, the above forward model is used to describe possible deviations in the amplitudes between the predicted multiples (represented by the vector, $\mathbf{f}$) and the multiples present in the observed data (the vector $\mathbf{g}$). Even though there is less of a direct link between the actual physics and this forward model, successful application of this approximation, where the differences between these two wavefield components are assumed to vary smoothly in phase space, has shown excellent results (Herrmann et al., 2008b).

APPROXIMATE FORWARD MODEL

After the appropriate global compensation for the stationary contribution of the matched filter (by e.g. a global matching procedure), the ΨDO in Equation 2 can be considered zero order and hence permits the following diagonal curvelet-domain decomposition (Herrmann et al., 2008a,b),

$$\mathbf{g} \approx \boldsymbol{C}^T \mathrm{diag}\{\mathbf{w}\}\boldsymbol{C}\mathbf{f}, \quad \{w\}_{\mu\in\mathscr{M}} > 0, \qquad (3)$$

with $\boldsymbol{C}$ the 2D discrete curvelet transform (see e.g. Candes et al., 2006) and $\mathbf{w}$ the curvelet-domain scaling vector and $\mathscr{M}$ the index set of curvelet coefficients. Since we are using the curvelet transform based on wrapping, which is a tight frame, we have $\boldsymbol{C}^T\boldsymbol{C} = \boldsymbol{I}\mathbf{d}$ and the transpose, denoted by the symbol ^{T}, equals the pseudo inverse.

In this approximate forward model, for which precise theoretical error estimates exist (Herrmann et al., 2008a), the two wavefields (or imaged wavefields) are matched by a simple

curvelet-domain scaling. This curvelet-domain scaling applies a location, scale and dip dependent amplitude correction. Since the matrix $\boldsymbol{B}$ is positive-definite, the entries in the scaling vector, $\mathbf{w}$, are positive. This approximate formulation of the forward model is the basis for our curvelet-domain matched filter.

CURVELET-DOMAIN MATCHED FILTERING

Equation 3 lends itself to an inversion for the unknown scaling vector. As both wavefields are known, our formulation minimizes the least-squares mismatch between the two of them. The following issues complicate the estimation of the scaling vector: (i) the undeterminedness of the forward model due to the redundancy of the curvelet transform—i.e., $\boldsymbol{C}\boldsymbol{C}^T$ is rank deficient; (ii) the risk of overfitting the data, which leads to unwanted artifacts such as incorrect amplitude corrections or inadvertent matching of primary energy, and (iii) the positivity requirement for the scaling vector. To address issues (i-ii), the following augmented system of equations is formed that relates the unknown scaling vector $\mathbf{w}$ to the augmented data vector, $\mathbf{d}$— i.e.,

$$\begin{bmatrix}\mathbf{g}\\ \mathbf{0}\end{bmatrix} = \begin{bmatrix}\boldsymbol{C}^T \operatorname{diag}\{\boldsymbol{C}\check{\mathbf{f}}\}\\ \gamma\boldsymbol{L}\end{bmatrix}\mathbf{w} \tag{4}$$

or $\mathbf{d} = \boldsymbol{F}_\gamma \mathbf{w}$. The scaling vector is found by minimizing the functional

$$J_\gamma(\mathbf{z}) = \frac{1}{2}\|\mathbf{d} - \boldsymbol{F}_\gamma e^{\mathbf{z}}\|_2^2, \tag{5}$$

where the substitution of $\mathbf{w} = e^{\mathbf{z}}$ (with the exponentiation taken elementwise) guarantees positivity (issue (iii)) of the solution (Vogel, 2002). This formulation seeks a solution fitting the vector, $\mathbf{g}$, with a smoothness constraint imposed by the sharpening operator $\boldsymbol{L}$, which for each scale penalize fluctuations amongst neighboring curvelet coefficients in the space and angle directions (see Herrmann et al., 2008a, for a detailed description). The amount of smoothing is controlled by the parameter γ. For increasing γ, there is more smoothness at the expense of overfitting the data (e.g., erroneously fitting the primaries). For a specific γ, the penalty functional in Equation 5 is minimized with respect to the vector $\mathbf{z}$ with the limited-memory BFGS (Nocedal and Wright, 1999) with the gradient

$$\operatorname{grad} J(\mathbf{z}) = \operatorname{diag}\{e^{\mathbf{z}}\}\left[\boldsymbol{F}_\gamma^T\left(\boldsymbol{F}_\gamma e^{\mathbf{z}} - \mathbf{d}\right)\right]. \tag{6}$$

Below, we discuss two applications of this curvelet-domain matched filter, each exploiting curvelet domain sparsity.

STABLE APPLICATION OF OUR MATCHED FILTER

We now show how to apply scaling stably. In the first example, we apply curvelet-domain scaling to correct for the normal operator of migration on a reflectivity model with conflicting dips. In the second example, we demonstrate how the matched filter improves Bayesian primary-multiple separation.

Seismic amplitude recovery: After migration, seismic images can be represented as $\mathbf{y} = \boldsymbol{\Psi}\mathbf{m}$ with $\mathbf{y}$ the migrated data, $\mathbf{m}$ the unknown reflectivity, and $\boldsymbol{\Psi}$ the demigration-migration operator. As long as this operator is zero order, the action of the normal operator can be replace by a curvelet-domain scaling. This suggests the following decomposition

$$\mathbf{y} = \boldsymbol{\Psi}\mathbf{m} \approx \boldsymbol{A}\boldsymbol{A}^T\mathbf{m} \tag{7}$$

with $\boldsymbol{A} = \boldsymbol{C}^T \operatorname{diag}\{\mathbf{w}^{1/2}\}$. The scaling coefficients are estimated with Equation 4 for $\mathbf{f} = \mathbf{r}$, $\mathbf{g} = \boldsymbol{\Psi}\mathbf{r}$ and $\mathbf{r}$, a reference vector close enough to the true image $\mathbf{m}$.

The decomposition in Equation 7 suggests the following forward model, $\mathbf{y} \approx \boldsymbol{A}\mathbf{x}_0$ with $\mathbf{x}_0$ a sparse set of curvelet coefficients. Following Herrmann et al. (2008a), we can now recover the seimic image by solving

$$\mathbf{P}_\varepsilon: \quad \begin{cases}\widetilde{\mathbf{x}} = \min_{\mathbf{x}} \|\mathbf{x}\|_1 & \text{subject to} \quad \|\mathbf{y} - \boldsymbol{A}\mathbf{x}\|_2 \le \varepsilon\\ \widetilde{\mathbf{m}} = \left(\boldsymbol{A}^T\right)^\dagger \widetilde{\mathbf{x}}\end{cases}$$

to within some user-defined tolerance level. To illustrate, the performance of our matched-filtering and subsequent amplitude recovery procedure, we consider a reflectivity consisting of a single cross. In this stylized example, we are particularly interested in showing the importance of imposing smoothness on the curvelet-scaling vector. As shown in Figure 1, the estimated scaling vector without regularization overfits the reference vector resulting in the emergence of a 'conflicting dip' (cf. Figure 1 (a) and (b) top row). In the case of no smoothing, an erroneous contribution emerges in the scales which can be attributed to overfitting. When smoothing is applied, this artifact is removed successfully, yielding good recovery for the amplitudes in Figure 2.

Bayesian primary-multiple separation: Ideally, the scaled multiples yielded by the above nonlinear least-squares problem, $\widetilde{\mathbf{z}} = \arg\min_{\mathbf{z}} J(\mathbf{z})$, could be subtracted from the total data directly. Unfortunately, the presence of noise in seismic imaging (see e.g. Herrmann et al., 2008a) and phase and kinematic errors in primary-multiple separation may interfere, rendering a separation based on the residual alone (as in SRME) ineffective. Following recent work by R. Saab and Herrmann (2007); Wang et al. (2008), we separate the primaries and multiples by solving the following sparsity-promoting program

$$\{\widetilde{\mathbf{x}}_1, \widetilde{\mathbf{x}}_2\} = \arg\min_{\mathbf{x}_1,\mathbf{x}_2} \lambda_1\|\mathbf{x}_1\|_{1,\mathbf{w}_1} + \lambda_2\|\mathbf{x}_2\|_{1,\mathbf{w}_2} \tag{8}$$

$$+ \quad \|\boldsymbol{A}\mathbf{x}_2 - \mathbf{b}_2\|_2^2 + \eta\|\boldsymbol{A}(\mathbf{x}_1 + \mathbf{x}_2) - \mathbf{b}\|_2^2, \tag{9}$$

where the vectors $\{\widetilde{\mathbf{x}}_1, \widetilde{\mathbf{x}}_2\}$ represent the estimates for the primaries and multiples, respectively, and where $\boldsymbol{A}$ is the curvelet synthesis matrix, $\{\mathbf{w}_1, \mathbf{w}_2\}$ positive weights, and $\{\mathbf{b}, \mathbf{b}_2\}$, the total data and the multiple prediction. Finally, the λ's and η are control parameters determining the sparsity of the solution and fits to the total data and multiple prediction. In this Bayesian formulation, both the multiple prediction and the weights depend on the curvelet-domain matching procedure.

FIELD DATA EXAMPLE

We test the above-described adaptive separation algorithm by examining real North Sea field dataset. The main purpose of this test is to study the improvement by curvelet-domain matching compared to results obtained with and estimate for the multiples yielded by optimized one-term SRME computed with a windowed-matched filter. This case is relevant for situations where the data quality does not permit iterative SRME or where the cost of multiple iterations of SRME is a concern. In either situation, the predicted multiples will contain amplitude errors, which may give rise to residual multiple energy

and dimmed primaries. We show that the proposed scaling by curvelet-domain matched filtering improves the estimation for the primaries as long the curvelet-to-curvelet variations for this scaling are sufficiently controlled by the smoothness constraint. Relaxation of this constraint may leads to overfitting and hence to inadvertent removal of primary energy.

Figure 3(a) contains the common-offset section (at offset 200 m) that we selected from a North Sea field dataset. Estimated primaries according to conventional SRME are plotted in Figure 3(b). Results where ℓ_2-matched filtering in the shot domain (Verschuur and Berkhout, 1997) is replaced by Bayesian thresholding (R. Saab and Herrmann, 2007) in the offset domain, are presented for a single offset in Figure 3(c), without scaling, and in Figure 3(d) with scaling. The scaled result is calculated for $\gamma = 0.3$. Juxtaposing the standard SRME and the curvelet-based results shows a removal of high-frequency clutter, which is in agreement with earlier findings reported in the literature. Moreover, primaries in the deeper part of the section (e.g. near the lower-two arrows in each plot) are much better preserved, compared to the standard-SRME result. Removal of the strong residual multiples in the shallow part, e.g. the first- and second-order water bottom multiples indicated by the arrows around 0.75 and 1.20 s, is particularly exciting. Due to the unbalanced amplitudes of the predicted multiples, both standard SRME and non-adaptive Bayesian thresholding are unable to eliminate these events. Our adaptive method, however, successfully removes these events by virtue of the curvelet-domain scaling. Compared to non-adaptive thresholding, residual multiples are better suppressed, while our adaptive scheme also leads to at least similar, but often even better, overall continuity and amplitude preservation of the estimated primaries. For example, improvements are visible in the lower-left corner of the sections (between offsets $[0-2000]$ m and times $[3.0-3.6]$ s), where low-frequency multiple residuals are better suppressed after curvelet-domain matched filtering (cf. Figure 3(c) and 3(d)), without deterioration of the primary energy. Finally, observe the improved recovery of primary energy at the lower arrow in Figure3(d), compared to the primary in Figure 3(c).

DISCUSSION AND CONCLUSIONS

In this paper, we presented a comprehensive method to compute the coefficients of a curvelet-domain matched filter and to apply the estimated filter through sparsity promotion. The stylized example with the conflicting dips underlined the importance of imposing phase-space smoothness while the field data example showed the merit of our method in the context of adaptive primary-multiple separation.

ACKNOWLEDGMENTS

The authors would like to thank Eric Verschuur for providing us with the SRME-primaries. We also would like to thank the authors of CurveLab for making their codes available. Norsk Hydro is thanked for making the field dataset available. This work was in part financially supported by the NSERC Discovery Grant (22R81254) of F.J.H. and CRD Grant DNOISE (334810-05), and was carried out as part of the SINBAD project with support, secured through ITF, from BG Group, BP, Chevron, ExxonMobil and Shell.

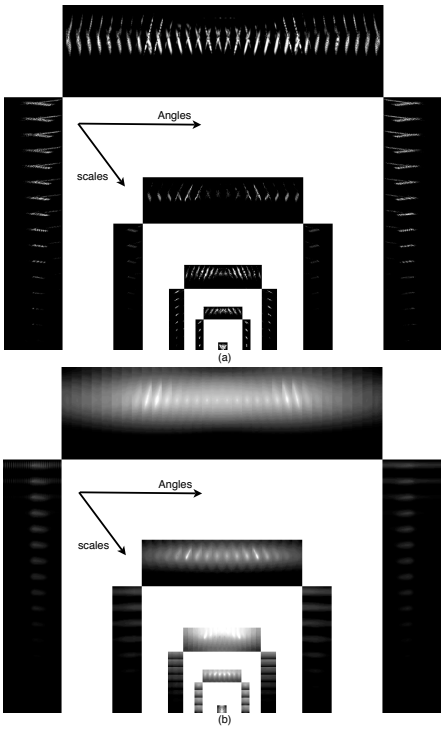

Figure 1: Curvelet-domain representation of the scaling vector obtained without **(a)**, and with a smoothing constraint, **(b)**. The different subimages represent the curvelet coefficients at different scales (coarsest in the center) and different angles. The location of the wedges roughly corresponds to the angle. Notice, the overfitting in **(a)**, leading to scaling at erroneous dips.

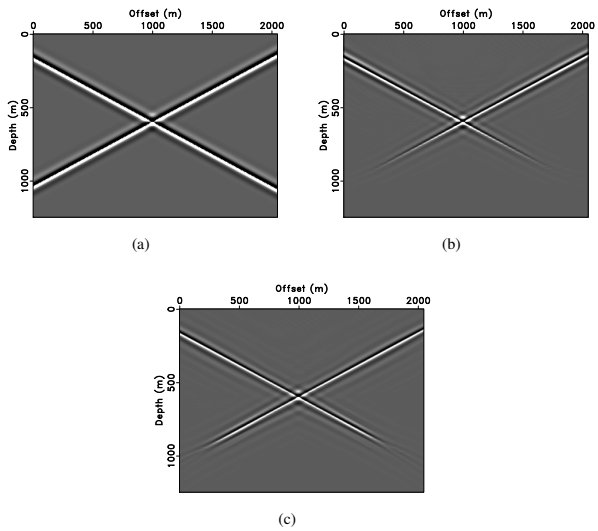

Figure 2: Curvelet-domain amplitude recovery according to $\mathbf{P}_{\mathcal{E}}$. **(a)** Original image with conflicting dips. **(b)** Migrated image. **(c)** Restored image.

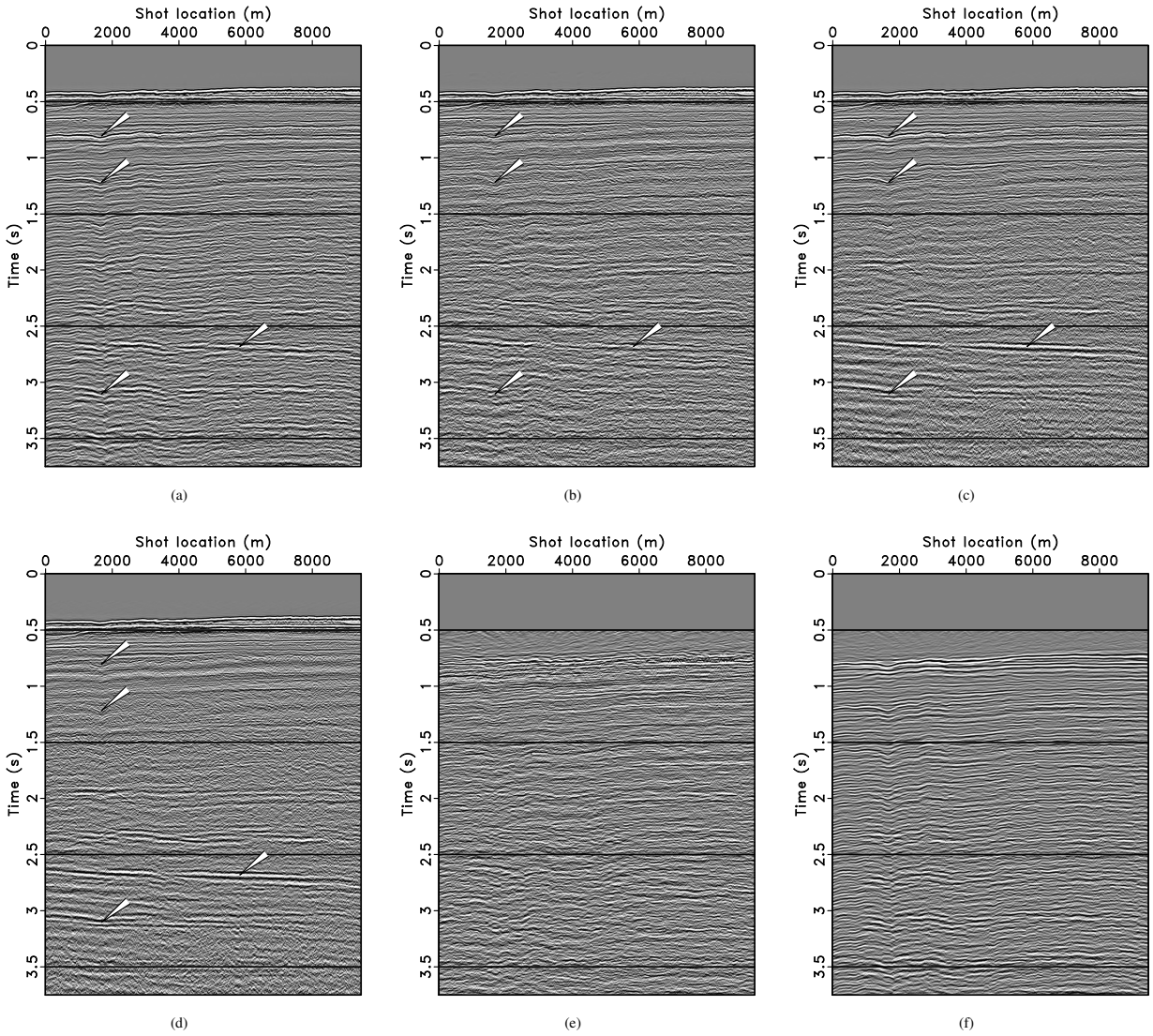

Figure 3: Adaptive curvelet-domain primary-multiple separation on real data. **(a)** Near-offset (200 m) section for the total data plotted with automatic-gain control. **(b)** Estimate for the primaries, yielded by optimized one-term SRME computed with a windowed-matched filter. **(c)** Estimate for the primaries, computed by Bayesian iterative thresholding with a threshold defined by $\mathbf{t} = |\boldsymbol{C}\check{\mathbf{b}}_2|$ with $\mathbf{b}_2$ the predicted multiples. **(d)** The same as **(c)** but now for the scaled (for $\gamma = 0.3$) threshold, i.e., $\mathbf{t} = |\mathrm{diag}\{\widetilde{\mathbf{w}}\}\boldsymbol{C}\mathbf{b}_2|$ with $\widetilde{\mathbf{w}} = \exp(\widetilde{\mathbf{z}})$. **(e)** The difference between SRME and matched filter. **(f)** Difference between the total data and the matched predicted primaries. Notice the improvement for the scaled estimate for the primaries, compared to the primaries yielded by SRME in **(b)** and by the Bayesian separation without scaling in **(c)**.

REFERENCES

Candes, E. J., L. Demanet, D. L. Donoho, and L. Ying, 2006, Fast discrete curvelet transforms: SIAM Multiscale Model. Simul., **5**, 861–899.

Guitton, A., 2004, Amplitude and kinematic corrections of migrated images for nonunitary imaging operators: Geophysics, **69**, 1017–1024.

Herrmann, F. J., P. P. Moghaddam, and C. C. Stolk, 2008a, Sparsity- and continuity-promoting seismic imaging with curvelet frames: Journal of Applied and Computational Harmonic Analysis, **24**, 150–173. (doi:10.1016/j.acha.2007.06.007).

Herrmann, F. J., D. Wang, and D. J. Verschuur, 2008b, Adaptive curvelet-domain primary-multiple separation. (Accepted for publication in Geophysics GEO-2007-0234).

Nocedal, J. and S. J. Wright, 1999, Numerical optimization: Springer.

R. Saab, D. Wang, O. Y. and F. Herrmann, 2007, Curvelet-based primary-multiple separation from a bayesian perspective: Presented at the SEG International Exposition and 77th Annual Meeting.

Symes, W. W., 2008, Approximate linearized inversion by optimal scaling of prestack depth migration: Geophysics, **73**, R23–R35. (10.1190/1.2836323).

Verschuur, D. J. and A. J. Berkhout, 1997, Estimation of multiple scattering by iterative inversion, part II: practical aspects and examples: Geophysics, **62**, 1596–1611.

Verschuur, D. J., A. J. Berkhout, and C. P. A. Wapenaar, 1992, Adaptive surface-related multiple elimination: Geophysics, **57**, 1166–1177.

Vogel, C., 2002, Computational Methods for Inverse Problems: SIAM.

Wang, D., R. Saab, O. Yilmaz, and F. J. Herrmann, 2008, Bayesian-signal separation by sparsity promotion: application to primary-multiple separation: Technical report, UBC Earth and Ocean Sciences Department. (TR-2008-1. (In revision.)).